COMMUNICATION

Water Oxidation Intermediates on Iridium Oxide Electrodes Probed by *In Situ* Electrochemical SHINERS

Khezar H. Saeed,[a] Mark Forster,[a] Jian-Feng Li,[b] Laurence J. Hardwick[a] and Alexander J. Cowan*[a]

Received 00th January 20xx,
Accepted 00th January 20xx

DOI: 10.1039/x0xx00000x

Shell-isolated nanoparticle-enhanced Raman spectroscopy (SHINERS) is applied to the study of a state-of-the-art water oxidation electrocatalyst, IrO_x, during oxygen evolution. The excellent sensitivity allows for *in-situ* detection of surface intermediate species during cyclic voltammetry. Features in the Raman spectrum are correlated with the redox behaviour of the electrode, demonstrating a way to study the mechanisms of electrocatalytic water splitting using equipment available in most laboratories.

Iridium oxide (IrO_x) is a well-studied water oxidation catalysts, with one of the lowest overpotentials for oxygen evolution and good stability even under acidic conditions.[1] While the low abundance and high cost of iridium make it impractical for very large scale (e.g. TW) deployment,[2] mechanistic studies on such an efficient catalyst are vital. They offer a chance to identify the design rules which can then be applied in the search for more abundant alternative materials. The electrochemical response of IrO_x has been studied in detail previously,[3,4] with an electrochromic effect being observed when cycling the material.[5] As a result, several UV-Vis spectroelectrochemical studies have been carried out,[6–8] correlating the population of an electronic state with λ_{max} of 450 nm with a water splitting intermediate. Additionally X-ray-based spectroscopies have been used to correlate an electrophilic $O^{\cdot-}$ species with the onset of oxygen evolution,[9,10] as well as identifying the formation of an Ir^{5+} species as a key step in the oxygen evolution reaction (OER).[11,12] A similar, highly valent, oxyl radical has previously been experimentally observed for $SrTiO_3$,[13] thought to be the intermediate preceding O-O bond formation. However, questions still remain, particularly relating to the role of solvation, the inhomogeneity of active sites and the potential dependent evolution of the IrO_x structure.

Identifying the chemical structure of any surface intermediates is a vital step in understanding the OER mechanism on IrO_x. *In situ* vibrational spectroscopy has proven to be useful for this, with Sivasankar *et al.*[14] reporting the discovery of an IrOOH (Scheme 1) mode at 830 cm^{-1} with a lifetime of several hundred ms on colloidal IrO_2. They utilise rapid-scan ATR-FTIR, with fast time resolution provided by exciting a $[Ru(bpy)_3]^{2+}$ visible light sensitiser with a 476 nm laser pulse, which then undergoes rapid charge transfer with the IrO_2 nanoparticles to drive water oxidation. Pavlovic *et al.* studied the electrocatalytic oxidation of water using IrO_x on a roughened Au substrate using Surface-Enhanced Raman Spectroscopy (SERS).[15] On a slower timescale (30 s per spectrum), they assigned a vibrational mode at 771 cm^{-1} to an electrochemically generated iridium oxo (Ir=O, Scheme 1) species, thought to be a key intermediate prior to O-O bond formation. These two findings would be consistent with the mechanism shown in Scheme 1, where the iridium oxo species is very long lived and the O-O bond formation is the rate limiting step, predicted to proceed via an oxyl radical (Scheme 1).[9,10,13] The short lifetime of the blue peroxide species suggests that oxygen evolution proceeds rapidly once this species is formed. This proposed mechanism is based on experiments using colloidal IrO_2 nanoparticles in solution and electrodeposited IrO_x thin films; a complete mechanism of water oxidation on a single type of iridium oxide remains elusive and many of the proposed further intermediates are yet to be experimentally observed on any IrO_x surface.

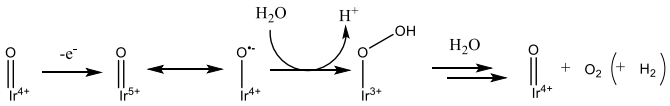

Scheme 1: Proposed mechanism for water oxidation at iridium centres based on observed and predicted intermediates in the existing literature.[10–12,14,15]

In situ Raman techniques are especially useful for aqueous systems as many of the proposed intermediates are expected to have vibrational modes below 1000 cm^{-1}, a region that is harder to probe experimentally using IR light due to severe attenuation of the light by water. Unfortunately, the use of SERS limits the choice of substrates to a handful of metal electrodes with a surface plasmon resonance in the visible region. Furthermore, the exposed SERS-substrate can significantly contribute to both the electrochemical and spectroscopic

[a] Stephenson Institute for Renewable Energy and the Department of Chemistry, University of Liverpool, Liverpool, L69 7ZD, UK, acowan@liverpool.ac.uk
[b] State Key Laboratory of Physical Chemistry of Solid Surfaces, College of Chemistry and Chemical Engineering, Xiamen University, Xiamen 361005, China
Electronic Supplementary Information (ESI) available: [details of any supplementary information available should be included here]. See DOI: 10.1039/x0xx00000x

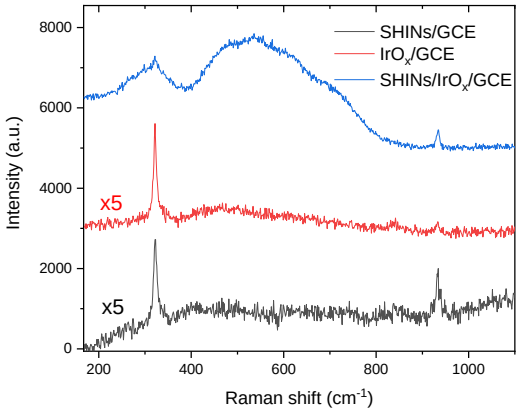

Figure 1: Stacked Raman spectra of the glassy carbon electrode system at 0.9 V (vs Ag/Ag^+) in 1 M $NaClO_4$, with the main IrOx feature (broad band between 400 and 800 cm^{-1}) being significantly enhanced in the presence of the SHINs. The sharp bands at 321 and 933 cm^{-1} correspond to CaF_2 (window material) and ClO_4^- (electrolyte) modes respectively. The full set of spectra for these systems can be found in Figures S5-S7.

response,[15] severely complicating analysis. Such challenges are universally present in studying electrocatalysts and an easily accessible method of *in situ* characterisation is sorely required for gaining mechanistic understandings, in real-time, of such electrocatalytic centres.[16]

SHINERS is a novel approach to SERS, where the enhancement is provided by nanoparticles encapsulated within an inert shell, which can be dropped onto the surface of almost any sample, allowing a wider range of materials and applications to be studied.[17] The inert shell eliminates concerns of the nanoparticle's metal core affecting the chemistry and is thin enough to still provide an enhanced Raman signal. Despite only being developed in the last decade, numerous applications of SHINERS have already been explored in the fields of electrochemistry,[18–26] bioanalysis,[27,28] and food safety[17], amongst others. These uses were highlighted in a recent review by Li *et al.*,[29] which discusses in detail the theory, development and varied applications of core-shell nanoparticle-enhanced Raman spectroscopy. Few studies have reported the use of SHINERS for studying water oxidation systems, with each monitoring processes occurring prior to catalysis. Huang *et al.* used the technique to follow structural changes on platinum single crystal surfaces, identifying vibrations of platinum peroxo and superoxo species prior to the onset of the oxygen evolution reaction (OER),[30] while Li *et al.* studied the oxidative reactions occurring at gold and copper electrodes preceding water oxidation.[31,32] Here, we expand on this work by detecting surface intermediates both prior to, and for the first time, during catalytic water splitting on state-of-the-art iridium oxide films deposited on (non-SERS-active) glassy carbon electrodes (GCE). This provides the demonstration of this simple technique to water oxidation mechanisms.

IrO_x was deposited in the manner previously described by Mallouk *et al.*, with Raman and electrochemical characterisation confirming its presence and activity. A simple drop-casting procedure was used to deposit the SiO_2 (2 nm) coated Au nanoparticle (55 nm) SHINs on the surface. Characterisation of the SHINs can be found in Figures S1-S3.

Figure 1 shows that the main iridium oxide feature between 400 and 800 cm^{-1}, corresponding to various Ir-O-Ir bend vibrations coupled to O-H vibrations,[33] is clearly enhanced in the presence of the SHINs and no additional peaks are observed in this spectral region from the SHINs themselves. Additionally, these spectra are taken *in situ*, under potentiostatic control (0.9 V, neutral 1 M $NaClO_4$), highlighting the ease of using SHINERS on different electrode surfaces. The presence of SHINs on the surface does not change the electrochemical response of the system (Figure S8). Iridium oxide is more active at higher pH,[15] so a larger surface density of active sites can be expected at more basic pH values, likely leading to more Raman scattering from any intermediates. The data presented in Figure 2 were collected at pH 10 as a balance between OER activity and stability of the silica shell of the SHINs, which are stable for greater than 30 minutes even at pH 12 (Figure S4).[34] The excellent sensitivity of the SHINERS measurements enabled collection of spectra while sweeping the potential towards water oxidation (5 mV s^{-1}, Figure 2). Structural changes along the way can be monitored by correlating changes in the Raman spectrum with features in the voltammogram.

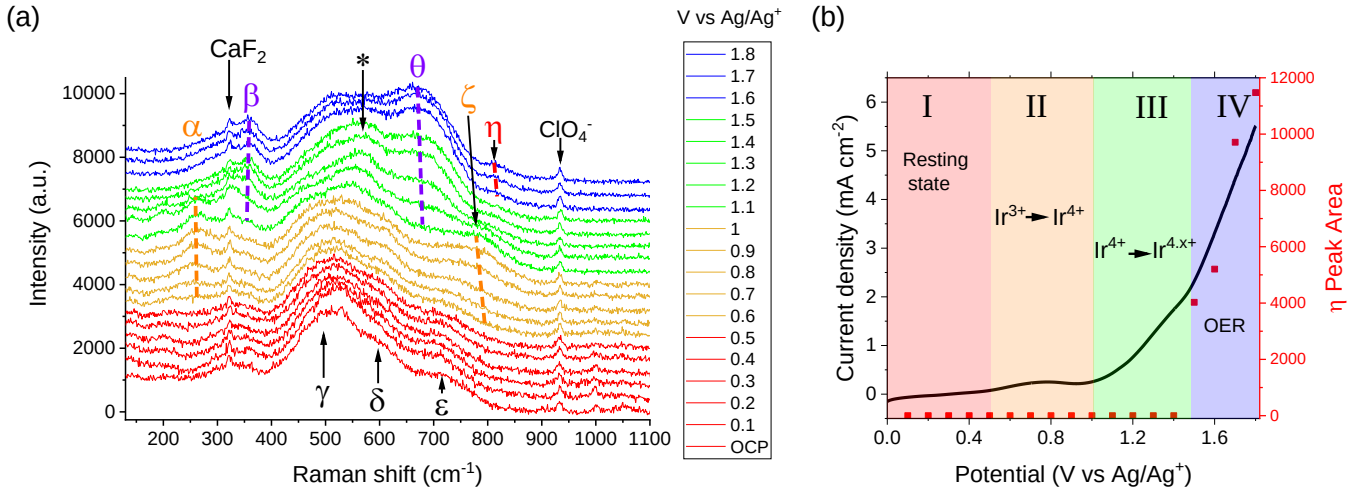

Figure 2: (a) Potential-dependent SHINER spectra (stacked) recorded during the (b) linear sweep voltammogram, overlaid with potential-dependence of the η peak area (Lorentzian peak fittings in Figure S11) of a SHINERS/IrOx/GCE system during a 5 mV s^{-1} linear sweep in 1 M $NaClO_4$ adjusted to pH 10 with NaOH.

The current-voltage response of the IrO_x film can be divided into 4 distinct regions (Figure 2 (b)), starting with near open circuit potentials (I), then the first oxidation from mostly Ir^{3+} to Ir^{4+} (II), oxidation from Ir^{4+} to Ir^{5+} (III) and finally OER conditions (IV).[3] Similarly, the SHINER spectra can be divided into four distinct groups, Figure 2 (a). The spectrum at open circuit potential (OCP, ~ 0.1 V vs Ag/Ag^+) is very similar to that reported by Pavlovic *et al.* using SERS, being dominated by the peaks labelled γ, δ and ε (the labelling of peaks α-η is used here to be consistent with prior literature).[33,35] Table 1 provides assignments of the Raman modes.

Table 1: Approximate Raman peak positions and assignments of IrO_x/GCE system (Figure 2), based on previous literature reports.[15,33]

Label	Peak Position (cm^{-1})	Assignment	Species
α	262	Ir-O-Ir twist	Ir^{4+}
β	357	Ir-O-Ir twist	$Ir^{4.x+}$
γ	504	Ir-O-Ir stretch	Ir^{4+}
δ	608	Ir-O-Ir stretch	Ir^{3+}
ε	719	Ir-O-Ir stretch	Ir^{4+}
ζ	773	Ir-O-Ir stretch	Ir^{4+}
θ	672	Ir-O-Ir stretch	$Ir^{4.x+}$
η	813 in H_2O 817 in D_2O	Ir=O stretch	$Ir^{4.x+}$

α and ζ are proposed to be the Ir-O-Ir twisting and stretching modes of Ir^{4+} oxides, respectively, as they grow in during region II and decrease in intensity in region III, concomitant with the appearance of β and θ. The Ir^{4+} centres are expected to be further oxidised in region III, suggesting that β & θ correspond to vibrations of this "pre-catalytic" $Ir^{4.x+}$ species. The smooth transition between α & β is extremely well-correlated with the 2nd oxidation of the iridium centres, which could indicate that they correspond to the same vibration, blue-shifted due to the change in metal oxidation state. Similar weak modes have previously been observed in the Raman spectra of amorphous IrO_2, however there is no consensus on their origin.[36–39] Alternatively, two modes around these frequencies have been previously assigned to Ir-O-Ir twisting vibrations by Pavlovic *et al.*,[15] though no such potential dependence was observed in their spectra. The proximity to gold oxide bands that may have been formed in this past SERS study prevented detailed study of their potential-dependent behaviour. Using electrochemically inert SHINs we can preclude the formation of gold oxide, allowing us to tentatively assign these bands to the twisting Ir-O-Ir modes of Ir^{4+} and $Ir^{4.x+}$ centres. Similarly, the peaks labelled ζ and θ also correlate with the two oxidations observed in the voltammogram and are assigned to the Ir-O-Ir stretching modes of Ir^{4+} and $Ir^{4.x+}$ centres, respectively, on the basis of comparison to previous Raman studies,[15,33] though they are labelled independently of these reports to highlight their clear potential dependence.

As observed in the literature, the E_g peak of rutile IrO_2 at 563 cm^{-1} (labelled *) also appears transiently in region III, implying the presence of different phases of iridium oxide within the material. The transition from the hydrous IrO_x structure to rutile IrO_2 has been described as a deactivation pathway in anodic iridium oxide films.[33] Interestingly, as we are carrying out experiments using confocal Raman microscopy, we are able to maintain study of a single region of the electrode throughout and we find that the formation of the rutile structure is not permanent and the spectrum after cycling back to OCP (Figure S9) largely resembles the initial spectrum, with no evidence of the Rutile IrO_2 band remaining.

Careful inspection of the Raman spectra shows the formation of a new band, η, at 815 cm^{-1} at the most positive potentials studied (region IV), Figure 3. It is striking that the potential-dependence of the peak area for this band directly correlates to the catalytic OER current, Figure 2 (b). η was previously assigned as the iridium-oxo intermediate by Pavlovic *et al.* at 771 cm^{-1} in their study, based on DFT modelling of iridium clusters. They predicted a vibrational mode at 829 cm^{-1} for the Ir=O stretch, though this mode can redshift significantly when a water molecule is placed nearby the cluster, hence the assignment of η at 771 cm^{-1} instead of 829 cm^{-1}. In our spectra, we assign η as the peak at 813 cm^{-1}, based both on similarity in position to the theoretical value (between 771 and 829 cm^{-1}) and since it is only present when a catalytic water oxidation current is being drawn. To investigate the observed Raman bands further, in particular η, the experiments were repeated in a D_2O-based (1 M $NaClO_4$, pD = 10) electrolyte, Figure S12. It is notable that no significant change in peak positions is observed, thus, any of the vibrational modes observed in this region are not likely to be (protonated) hydroxides or peroxides. This is not entirely surprising as the mechanism proposed in Scheme 1 only contains one species with an O-H bond, the peroxide intermediate (labelled blue), which was shown to be very short-lived by the rapid-scan FTIR experiments.[14] A minor shift is observed in the position of η, though this is in-line with the assignment to an Ir=O stretch which is solvated by H_2O/D_2O.[15]

In conclusion, we have demonstrated the use of SHINERS to probe the surface mechanism of electrocatalytic water oxidation by IrO_x, during voltage-sweep measurements, in real-time. In using inert coated Au nanoparticles, we avoid complications from using one of the limited number of SERS-active substrates. The sensitivity of the technique, along with speed of acquisition offers an exciting opportunity to the water splitting and solar fuels community. For example the

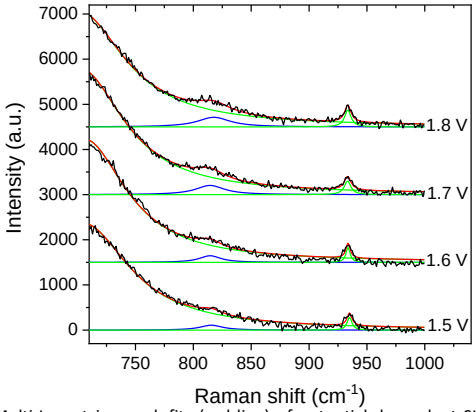

Figure 3: Multi-Lorentzian peak fits (red line) of potential-dependent SHINER spectra (black, raw data) of IrO_x/GCE surface during a 5 mV s^{-1} LSV in 0.1 M $NaClO_4$. The individual Lorentzian peaks are in green except for η shown in blue (*ca.* 815 cm^{-1}). Justification of the fitting procedure can be found alongside Figure S10.

inhomogeneity of electrochemical behaviour of IrO_x films, readily visualised by the electrochromic behaviour in Figure S11, has long been a topic of interest to the field and SHINERS offers the opportunity to map, in real-time, the changing chemistry of the electrode surface. As such, the technique is ideal for studying other promising (photo-)electrode materials for water splitting and initial work is in progress applying SHINERS to Fe_2O_3 and TiO_2 electrodes. Finally, we note the potential for coupling this highly sensitive technique to time-resolved potential-step and photo-initiated measurements and experiments are underway in our laboratory with the aim of detecting the transient oxyl and peroxo species suggested in Scheme 1.

Conflicts of interest

There are no conflicts to declare.

The authors acknowledge T. Galloway and A. Grzedowski (University of Liverpool) and J.-C. Dong, Y.-H. Wang and J. Xu (Xiamen University) for assistance in synthesis, stability testing and *in situ* electrochemical SHINERS. Support from EPSRC grants EP/N032888/1, EP/K006851/1 and EP/P034497/1, EPSRC Global Challenges Research Fund (GCRF) Institutional Award and Royal Society Travel Grant is also gratefully acknowledged.

References

1 C. C. L. McCrory, S. Jung, J. C. Peters and T. F. Jaramillo, *J. Am. Chem. Soc.*, 2013, **135**, 16977–16987.
2 J. Kibsgaard and I. Chorkendorff, *Nat. Energy*, 2019, **4**, 430–433.
3 P. Steegstra, M. Busch, I. Panas and E. Ahlberg, *J. Phys. Chem. C*, 2013, **117**, 20975–20981.
4 P. Steegstra and E. Ahlberg, *Electrochim. Acta*, 2012, **76**, 26–33.
5 S. Gottesfeld, J. D. E. McIntyre, G. Beni and J. L. Shay, *Appl. Phys. Lett.*, 1978, **33**, 208–210.
6 G. S. Nahor, P. Hapiot, P. Neta and A. Harriman, *J. Phys. Chem.*, 1991, **95**, 616–621.
7 H. Ooka, Y. Wang, A. Yamaguchi, M. Hatakeyama, S. Nakamura, K. Hashimoto and R. Nakamura, *Phys. Chem. Chem. Phys.*, 2016, **18**, 15199–15204.
8 H. Ooka, A. Yamaguchi, T. Takashima, K. Hashimoto and R. Nakamura, *J. Phys. Chem. C*, 2017, **121**, 17873–17881.
9 C. Massué, V. Pfeifer, M. van Gastel, J. Noack, G. Algara-Siller, S. Cap and R. Schlögl, *ChemSusChem*, 2017, **10**, 4786–4798.
10 V. A. Saveleva, L. Wang, D. Teschner, T. Jones, A. S. Gago, K. A. Friedrich, S. Zafeiratos, R. Schlögl and E. R. Savinova, *J. Phys. Chem. Lett.*, 2018, **9**, 3154–3160.
11 Y. Mo, I. C. Stefan, W. Bin Cai, J. Dong, P. Carey and D. A. Scherson, *J. Phys. Chem. B*, 2002, **106**, 3681–3686.
12 H. G. Sanchez Casalongue, M. L. Ng, S. Kaya, D. Friebel, H. Ogasawara and A. Nilsson, *Angew. Chemie Int. Ed.*, 2014, **53**, 7169–7172.
13 D. M. Herlihy, M. M. Waegele, X. Chen, C. D. Pemmaraju, D. Prendergast and T. Cuk, *Nat. Chem.*, 2016, **8**, 549–555.
14 N. Sivasankar, W. W. Weare and H. Frei, *J. Am. Chem. Soc.*, 2011, **133**, 12976–12979.
15 Z. Pavlovic, C. Ranjan, M. Van Gastel and R. Schlögl, *Chem. Commun.*, 2017, **53**, 12414–12417.
16 F. Song, L. Bai, A. Moysiadou, S. Lee, C. Hu, L. Liardet and X. Hu, *J. Am. Chem. Soc.*, 2018, **140**, 7748–7759.
17 J. F. Li, Y. F. Huang, Y. Ding, Z. L. Yang, S. B. Li, X. S. Zhou, F. R. Fan, W. Zhang, Z. Y. Zhou, D. Y. Wu, B. Ren, Z. L. Wang and Z. Q. Tian, *Nature*, 2010, **464**, 392–395.
18 T. A. Galloway and L. J. Hardwick, *J. Phys. Chem. Lett.*, 2016, **7**, 2119–2124.
19 M. M. Liang, Y. H. Wang, R. Shao, W. M. Yang, H. Zhang, H. Zhang, Z. L. Yang, J. F. Li and Z. Q. Tian, *Electrochem. commun.*, 2017, **81**, 38–42.
20 G. Cabello, X. J. Chen, R. Panneerselvam and Z. Q. Tian, *J. Raman Spectrosc.*, 2016, **47**, 1207–1212.
21 Ji-Yang, J.-C. Dong, V. V. Kumar, J.-F. Li and Z.-Q. Tian, *Curr. Opin. Electrochem.*, 2017, **1**, 16–21.
22 C. Y. Li, J. C. Dong, X. Jin, S. Chen, R. Panneerselvam, A. V. Rudnev, Z. L. Yang, J. F. Li, T. Wandlowski and Z. Q. Tian, *J. Am. Chem. Soc.*, 2015, **137**, 7648–7651.
23 A. J. Cowan and L. J. Hardwick, *Annu. Rev. Anal. Chem.*, 2019, **12**, 323–346.
24 T. A. Galloway, J.-C. Dong, J.-F. Li, G. Attard and L. J. Hardwick, *Chem. Sci.*, 2019, **10**, 2956–2964.
25 L. Cabo-Fernandez, D. Bresser, F. Braga, S. Passerini and L. J. Hardwick, *Batter. Supercaps*, 2019, **2**, 168–177.
26 T. A. Galloway, L. Cabo-Fernandez, I. M. Aldous, F. Braga and L. J. Hardwick, *Faraday Discuss.*, 2017, **205**, 469–490.
27 L. Lin, X. Tian, S. Hong, P. Dai, Q. You, R. Wang, L. Feng, C. Xie, Z. Q. Tian and X. Chen, *Angew. Chemie - Int. Ed.*, 2013, **52**, 7266–7271.
28 D. Drescher, I. Zeise, H. Traub, P. Guttmann, S. Seifert, T. Büchner, N. Jakubowski, G. Schneider and J. Kneipp, *Adv. Funct. Mater.*, 2014, **24**, 3765–3775.
29 J. F. Li, Y. J. Zhang, S. Y. Ding, R. Panneerselvam and Z. Q. Tian, *Chem. Rev.*, 2017, **117**, 5002–5069.
30 Y. F. Huang, P. J. Kooyman and M. T. M. Koper, *Nat. Commun.*, 2016, **7**, 1–7.
31 C. Li, J. Dong, X. Jin, S. Chen and R. Panneerselvam, 2015, 8–11.
32 N. Bodappa, M. Su, Y. Zhao, J.-B. Le, W.-M. Yang, P. Radjenovic, J.-C. Dong, J. Cheng, Z.-Q. Tian and J.-F. Li, *J. Am. Chem. Soc.*, 2019, **141**, 12192–12196.
33 Z. Pavlovic, C. Ranjan, Q. Gao, M. van Gastel and R. Schlögl, *ACS Catal.*, 2016, **6**, 8098–8105.
34 S. H. Lee, I. Rusakova, D. M. Hoffman, A. J. Jacobson and T. R. Lee, *ACS Appl. Mater. Interfaces*, 2013, **5**, 2479–2484.
35 Z. Pavlovic, C. Ranjan, M. van Gastel and R. Schlögl, *Chem. Commun.*, 2017, **53**, 12414–12417.
36 S. Thanawala, D. G. Georgiev, R. J. Baird and G. Auner, *Thin Solid Films*, 2007, **515**, 7059–7065.
37 A. Avila-García, G. Romero-Paredes and R. Peña-Sierra, *Progr. Abstr. B. - 2010 7th Int. Conf. Electr. Eng. Comput. Sci. Autom. Control. CCE 2010*, 2010, 537–540.
38 P. C. Liao, C. S. Chen, W. S. Ho, Y. S. Huang and K. K. Tiong, *Thin Solid Films*, 1997, **301**, 7–11.
39 S. Musić, S. Popović, M. Maljković, Z. Skoko, K. Furić and A. Gajović, *Mater. Lett.*, 2003, **57**, 4509–4514.

